A Graph-Based Optimization Approach for Resilient EV Rerouting in Disrupted Charging Networks

Md Rakibul Ahasan*, Shahriar Rahman Fahim†, Rachad Atat‡, and Abdulrahman Takiddin*
*Department of Electrical and Computer Engineering, Florida State University, Tallahassee, FL, USA
†Department of Electrical and Computer Engineering, Texas A&M University, College Station, TX, USA
‡Computer Science and Mathematics Department, Lebanese American University, Beirut, Lebanon

***Abstract*—The growing adoption of electric vehicles (EVs) increases the demand for a reliable and efficient charging infrastructure. Unexpected disruptions at electric vehicle charging stations (EVCSs) can negatively impact traffic flow and energy distribution. Traditional EV rerouting strategies to EVCS are limited by their static nature and fail to consider the interdependence between transportation and power distribution networks. Thus, traditional rerouting strategies are unable to effectively reroute EVs during EVCS disruptions that might occur due to maintenance, lack of public EVCS, or power unavailability, leading to congestion, increased travel time, and energy inefficiencies. In this paper, we propose a graph-based rerouting framework that integrates transportation and power networks to dynamically redirect EVs from disrupted to functional EVCSs while accounting for EVCS-to-EVCS distance, station capacity, and route capacity. The proposed method incorporates three years of travel monitoring analysis system traffic data with a synthetic power distribution network to capture realistic operating conditions. We introduce the EV rerouting with disruptions and capacity constraints (EVR-DC) algorithm, which incorporates system-level constraints and enables decentralized decision-making under disruptions. Our results show that the proposed approach reduces disrupted EVCS congestion by 73% within an hour and maintains an annual EV user rerouting satisfaction rate of 86%, demonstrating the effectiveness of the proposed method in enhancing the resilience of EV charging infrastructure against disruptions.**

***Index Terms*—Charging stations, disruption, electric vehicles, optimization, rerouting, transportation networks.**

I. Introduction

The widespread adoption of electric vehicles (EVs) in urban freight transport is driven by the urgent need to mitigate greenhouse gas emissions and reduce reliance on fossil fuels [1]. Technological advancements, including vehicle-to-grid integration, have facilitated multiple fast-charging events during vehicle journeys, making EVs increasingly viable for commercial applications [2], [3]. Government policies and incentives further accelerate the transition from conventional vehicles to EVs, particularly in response to urban air pollution concerns and the necessity for sustainable solutions [4]. The growth of EVs also presents several significant challenges, including the need for an efficient and ubiquitous charging infrastructure [5]. The planning and deployment of electric vehicle charging stations (EVCSs) must consider spatial constraints, high-power demand, and grid reliability to facilitate the integration of EVCSs into the grid [6]. Recent studies on dynamic power systems further emphasize that ensuring grid reliability under evolving topologies requires resilient graph-based formulations [7], [8]. Moreover, an on-the-go EV monitoring systems using onboard diagnostics to support battery state-of-health estimation are critical for informed rerouting and energy management [9]. Despite the ongoing expansion of charging infrastructure, the average reliability score of EVCS in the U.S. is around 78%, implying that one out of five EVCSs might not be operational at a given time [10]. To address this, we propose an optimization strategy for EV rerouting to functional EVCS using real-time data and advanced decision-making algorithms to enhance system resilience and user satisfaction.

We acknowledge that charging port availability is increasingly provided through existing EVCS mobile applications. However, such availability information is often limited to charging provider-owned mobile applications and lacks interoperability across broader, heterogeneous networks [11]. Moreover, real-time availability data may not reflect unanticipated disruptions, communication delays, or cascading failures affecting adjacent EVCSs [3]. In contrast to routing decisions based solely on static or ideal availability, our proposed framework addresses dynamic rerouting under such post-departure disruptions, accounting for EVCS distance, capacity, and route constraints where prior availability proves insufficient.

A. Related Work

The EV routing problem (EVRP) differs from traditional vehicle routing problems by considering en-route charging and the availability of EVCS [12]. To address the EVRP, researchers have developed various optimization-based strategies. For example, a greedy randomized adaptive search algorithm achieved distance reductions of up to 56% but exhibited poor scalability when extended to larger networks [13]. A modified genetic algorithm (GA) that incorporated flexible crossover and pre-post mutation enhanced local search capabilities and produced an optimal solution with 39% faster EV routing decision than the traditional, however, ignored realistic EV rerouting scenarios [14]. A tabu search (TS) algorithm is used to optimize delivery routes by considering battery constraints. TS reduced EV routing simulation time, leading to faster EV routing decisions by 90%. However, the evaluation is limited to a small EV network of three EVs [15]. Moreover, a mixed-integer linear programming model (MILP) integrated

TABLE I
EVRP SYSTEM SETTINGS, METRIC, RESULTS, AND LIMITATIONS ACROSS REFERENCES

Model	System Settings						Goal	Result	Limitation
	EVCS Location	EV Battery Capacity	Route Distance	EVCS Capacity	Penalty Cost	EVCS Disruption			
GA [14]	✓	-	✓	-	-	-	Faster rerouting to EVCS convergence	39% improvement	Missing realistic EV routing scenario
TS [15]	✓	✓	✓	-	-	-	Improve EV routing decision time	90% improvement	Small EV network for routing
MILP [16]	✓	✓	✓	-	-	-	Improve EV energy consumption	23% improvement	High computational complexity
LNSA [17]	✓	✓	✓	-	-	-	Improve routing optimization gain	81% improvement	Simplistic routing scenario
Proposed work	✓	-	✓	✓	✓	✓	Improve rerouting satisfaction rate	86% satisfaction	No forecasting of disruption

with vehicle motion dynamics, regenerative braking, and 3D road geometry was proposed to optimize both EV routing and EVCS placement. While the MILP model reduced EV energy consumption by up to 23%, it increased EVCS-to-EVCS travel distance by 26%. The MILP model also faced high computational complexity when dealing with a large-scale EV network [16]. Conversely, an improved large neighborhood search algorithm was employed across various EVRP instances, gaining optimal routing solutions in 81% of the instances; however, the computational time increased as the complexity of the routing scenarios grew [17].

In Table I, we present a summary of the system settings, performance metrics, experimental results, and limitations of relevant studies. The system settings include the physical locations of EVCSs, EV battery capacity, route distance between EVCS nodes, the capacity of each EVCS to accommodate incoming EVs, the penalty cost in the routing objective function, and whether an EVCS is disrupted or not. Table I also shows that different studies adopt diverse evaluation criteria, making it difficult to establish a common comparison ground. In our proposed work, we incorporate all system settings except for the EV battery capacity. The key performance metric of our work is the rerouting satisfaction rate, $\mathcal{R}$, defined as the ratio of the number of EVs successfully rerouted at alternative stations to the total number of EVs affected by the disruption.

B. Problem Definition and Contributions

As EV penetration increases, the number of EVCS deployed across transportation networks continues to rise. However, such a growing infrastructure introduces new operational challenges, particularly in the form of traffic congestion and service disruptions. EVCS may become temporarily unavailable due to maintenance, equipment failure, or fluctuations in power supply. These disruptions not only reduce charging availability but also affect traffic flow and overall energy efficiency. To manage these challenges, rerouting strategies are essential for guiding EVs from non-operational EVCSs to functional alternatives. Traditional rerouting methods [13] - [17] are often static and fail to account for the dynamic interplay between the transportation network and the underlying power distribution system. They typically neglect key system constraints such as EVCS capacity, road-level traffic conditions, and inter-EVCS connectivity, resulting in inefficient rerouting decisions under real-time disruptions. To address such limitations, we propose a graph-based rerouting framework that dynamically models the EVCS network under disruption scenarios. The contributions of our research are summarized next.

- Firstly, we formulate a disruption-aware EV rerouting problem that accounts for EVCS-to-EVCS distance, EVCS capacity, and route-level flow constraints. The problem is designed to operate over a coupled transportation and power network, enabling realistic and system-aware decision-making.
- Secondly, we propose the EV rerouting with disruptions and capacity constraints (EVR-DC) algorithm, which dynamically redirects EVs from disrupted to functional EVCS. Our approach integrates three years of real-world traffic data across 305 EVCS locations and achieves an annual EV user rerouting satisfaction rate of 86%.
- Thirdly, our proposed algorithm limits rerouting within a two-hop neighborhood to ensure feasibility and reduce computational burden. In hourly simulations, the EVR-DC algorithm decreases congestion at disrupted EVCS by 73%, demonstrating both scalability and practical efficiency under constrained network conditions.

The remainder of this paper is organized as follows. Section II outlines the system overview. Section III covers the dataset and preprocessing. Section IV presents the rerouting objective and solution. Section V analyzes our experimental results. Section VI concludes the paper.

II. SYSTEM OVERVIEW

Our system model, illustrated in Fig. 1, consists of a power system and a transportation system. The top part of Fig. 1 reflects the power bus system represented by a graph $\mathcal{G}_{\text{bus}} = (\mathcal{B}, \mathcal{T})$, where $\mathcal{B}$ is the set of buses in the power system, and $\mathcal{T}$ represent the transmission line between buses. The branch power flow states that the power $P^{a,b}$ flowing into bus b from its parent bus a, expresses as

$$P^{a,b} = \sum_{\beta \in \Omega} P^{b,\beta} + P^{b}_{\text{res}} + P^{b}_{\text{inc}} + P^{b}_{\text{EVCS}} + P^{a,b}_{\text{loss}}, \quad b \neq 1, \tag{1}$$

must equal the sum of the power sent to all downstream buses $\beta \in \Omega$ (Ω is the set of buses where $b \notin \Omega$), where P^{b}_{res}, P^{b}_{inc},

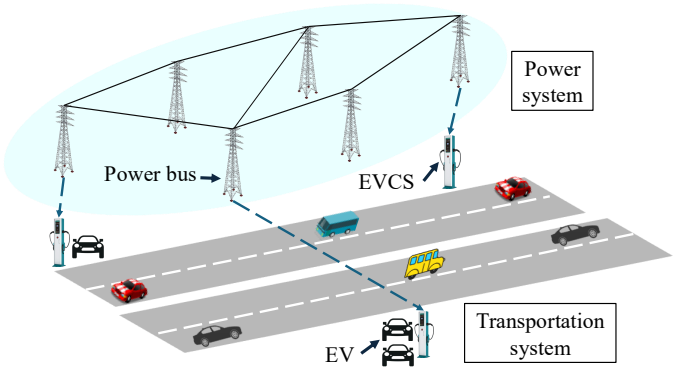

Fig. 1. An illustration of the coupled power and transportation system model

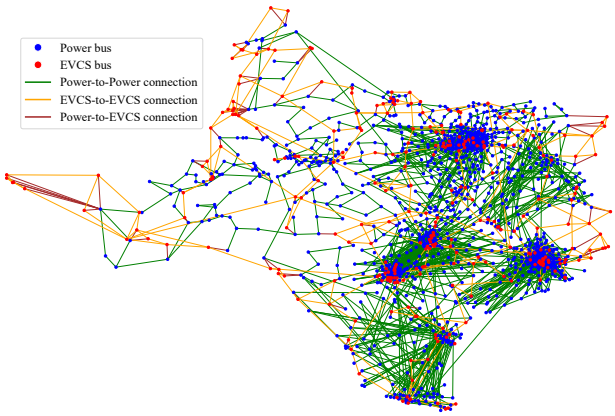

Fig. 2. Undirected connected graph structure for power and EVCS nodes

and P^{b}_{EVCS} denote the power consumed by residential loads, industrial loads, and the EVCS. $P^{a,b}_{\text{loss}}$ denotes the power loss over the transmission line. The bottom part of Fig. 1 represents the transportation network, which is defined as an undirected graph $\mathcal{G}_{\text{EVCS}} = (\mathcal{M}, \mathcal{E})$, where $\mathcal{M}$ is the set of EVCS nodes and $\mathcal{E}$ is the set of routes connecting them. The route set $\mathcal{E}$ is constructed based on the minimum Haversine distance, which computes the shortest great-circle distance between the EVCSs [18]. In between node pairs in $\mathcal{M}$, $\mathcal{E}$ is represented as

$$\mathcal{E} = (i,j) \in \mathcal{M} \times \mathcal{M} \;\; i \neq j, \;\; d^{i,j} = \min_{\alpha \in \mathcal{M}} \text{Haversine}(i, \alpha) \quad (2)$$

where $d^{i,j}$ is the Haversine distance between EVCS i and j, and each route $(i,j) \in \mathcal{E}$ represents a bidirectional (two-way) road, α is the set of intermediate EVCS between routes. To establish a coupled connection between the EVCS network and power bus system, each EVCS node $i \in \mathcal{M}$ in the transportation graph $\mathcal{G}_{\text{EVCS}}$ is linked to its geographically nearest power bus $a \in \mathcal{B}$ from the power graph $\mathcal{G}_{\text{bus}}$. This connection is based on the minimum Haversine distance [1]. The resulting set of interconnections is defined as

$$\mathcal{Z} = (i,a) \in \mathcal{M} \times \mathcal{B} \mid a = \arg\min_{b \in \mathcal{B}} \text{Haversine}(i, b) \quad (3)$$

Our system model formulation ensures that each EVCS is connected to the most spatially efficient power bus, allowing for realistic modeling of infrastructure integration between transportation and power buses.

III. Dataset Description

We integrate traffic and power data to build the graph-based EVCS network. The traffic data is sourced from a travel monitoring analysis system (TMAS) based in Texas, U.S., where state highway agencies collect traffic counts using both temporary and continuous methods in EVCS geographical coordinates, with continuous traffic density data reported monthly to the federal highway administration [19]. From the TMAS monthly measurements, we extract the existing hourly and yearly resolution data for 2021 to 2023. For a realistic EV traffic analysis, we assume that 30% of the total traffic comprises EVs [20] and that 5% of these EVs require charging at an EVCS [21]. Consequently, our dataset includes three years of hourly traffic density records for 305 EVCSs, with IDs ranging from $S0$ to $S304$. In parallel, the power bus measurement and geographical data are derived from ACTIVSg2000, a synthetic 2000-bus power system model of Texas state [22]. The 2000-bus system model is built using publicly available information and statistical analysis of real power systems, ensuring that the generation and load profiles closely mirror those in actual power systems, with detailed measurements of power at each power bus. Referring to Eq. 2 and Eq. 3 and using the geographical coordinates of EVCS and power bus, we construct a combined graph of power bus and EVCS as shown in Fig. 2. Consequently, the EVCS network is represented by a 305×305 adjacency matrix A, with each element storing the Haversine distance between a pair of EVCS nodes. Based on this connection, the capacity allocated to each EVCS is determined by the available power (P_{EVCS}) at the connected bus, calculated as the total available power (P_{total}) minus the residential (P_{res}) and industrial (P_{inc}) load demands, i.e.,$P_{\text{EVCS}} = P_{\text{total}} - P_{\text{res}} - P_{\text{inc}}$ [23], divided by the EV charging demand that is modeled as a fraction of the battery capacity, typically ranging from 20% to 80% [24]. The route capacity is computed as the Haversine distance divided by the sum of a 5 meter vehicle length and a 2.5 meter vehicle spacing [25].

IV. Rerouting Objective

The traffic density at disrupted and functional nodes is denoted by $\mathcal{Q}_v$ and $\mathcal{N}_v$, respectively, where v is the incoming EV at hour h and $\mathcal{Q} \subseteq \mathcal{M}$, $\mathcal{N} \subseteq \mathcal{M}$ represents the disrupted and functional nodes set. The capacity of each functional EVCS is represented by $\mathcal{N}_c$. In this formulation, each node $i \in \mathcal{Q}$ refers to a disrupted EVCS, each node $j \in \mathcal{N}$ denotes a functional destination EVCS, and $k \in \mathcal{M}$ represents an intermediate node used to facilitate decision-making in the EV rerouting process. On the contrary, $x^{i,j}$ represents the variable where the EV is routed from a disrupted node to a functional node without any intermediate hop k. $x^{i,k,j}$ represents the EV is routed from a disrupted node to a functional node with intermediate hop k. $\mathcal{E}^{i,j}_{c}$ represents the cumulative route capacity between the disrupted node and to functional node.

A. Disruption on Most Vulnerable EVCS

Highly utilized EVCSs are inherently more susceptible to disruptions [26]. Under extreme weather conditions or network stress, such EVCS may become unavailable for service [27]. To model such disruptions, we first compute the traffic density $\mathcal{M}_v^i$ at each EVCS node $i \in \mathcal{M}$, where $\mathcal{M}$ denotes the set of all EVCS nodes. We introduce a disruption budget W, which allows for the disruption of up to q EVCS nodes with the highest traffic densities. Then, we select a subset $\mathcal{Q} \subseteq \mathcal{M}$ as

$$\mathcal{Q} = \text{Top-}q\left(\{\mathcal{M}_v^i : i \in \mathcal{M}\}\right), \quad \text{with } |\mathcal{Q}| = q, \quad q \leq W \tag{4}$$

In our simulations, we set $W = 10$, thus identifying the 10 most heavily utilized EVCS nodes as vulnerable to disruption. EVs initially associated with these disrupted nodes must then be dynamically rerouted to available alternatives.

B. EV Rerouting Cost Minimization

The EV rerouting cost minimization objective function $\mathcal{U}$ consists of three terms. The first term, weighted by w_1, penalizes longer routes by considering the travel distance $d^{i,j}$ for each chosen route, reflecting that longer detours increase EV energy consumption and prolong user waiting times [28]. The second term, with weight w_2, penalizes high loads on an EVCS by using the ratio $\mathcal{Q}_v^i/\mathcal{N}_c^j$, which measures the demand from a disrupted EVCS relative to the available capacity of a functional EVCS, thereby preventing excessive queuing delays and avoiding potential service denials due to EVCS overutilization [29]. The third term, weighted by w_3, addresses route capacity by using the ratio $\mathcal{Q}_v^i/\mathcal{E}_c^{i,j}$, which indicates how much of a route capacity is utilized, thereby reducing route congestion, preventing network bottlenecks, and preserving overall system reliability [29]. In our implementation, each LP solve treats EVCS capacities N_c^j as fixed; after obtaining the optimal routing, we update N_c^j to reflect incoming demand. To determine the weights w_1, w_2, w_3 in the optimization objective, we apply the analytic hierarchy process (AHP). Simulations are carried out across 15 hourly routing scenarios over five days, and the weight combination $(w_1,\ w_2,\ w_3) = (0.188,\ 0.623,\ 0.188)$ is found to yield the lowest total routing cost under Eq. 5. The resulting pairwise comparison matrix satisfies the AHP consistency criterion, yielding a consistency ratio of $\mathrm{CR} = 0.05$, which indicates a high level of logical coherence in the weight selection, as it falls well below the accepted threshold of 0.10. The formulation of $\mathcal{U}$ is defined as

$$\mathcal{U} = \min \Bigg[\sum_{(i,j)\in\mathcal{E}} w_1\, x^{i,j}\, d^{i,j} + \sum_{i\in\mathcal{Q}} \sum_{j\in\mathcal{N}} w_2\, x^{i,j}\, \frac{\mathcal{Q}_v^i}{\mathcal{N}_c^j} + \sum_{(i,j)\in\mathcal{E}} w_3\, x^{i,j}\, \frac{\mathcal{Q}_v^i}{\mathcal{E}_c^{i,j}} \Bigg] \tag{5}$$

The constraints of the objective function $\mathcal{U}$ are as follows: *Demand fulfillment*: The demand of each disrupted node must be met by rerouting the EV, ensuring at least 90% of the original demand is satisfied, such that

$$\sum_{j\in\mathcal{N}} x^{i,j} + \sum_{k\in\mathcal{M}} \sum_{j\in\mathcal{N}} x^{i,k,j} = 0.9 * \mathcal{Q}_v \quad ;\forall i \in \mathcal{Q} \tag{6}$$

Route capacity constraints: The number of EVs rerouted over each route must not exceed its capacity, i.e.,

$$\sum_{i\in\mathcal{Q}} \sum_{j\in\mathcal{N}} x^{i,j} \leq \mathcal{E}_c^{i,j} \quad ;\forall (i,j) \in \mathcal{E} \tag{7}$$

Node capacity constraints: The total incoming traffic at each destination node must not exceed its capacity, i.e.,

$$\sum_{i\in\mathcal{Q}} \sum_{j\in\mathcal{N}} x^{i,j} + \sum_{i\in\mathcal{Q}} \sum_{k\in\mathcal{M}} \sum_{j\in\mathcal{N}} x^{i,k,j} \leq \mathcal{N}_c \quad ;\forall j \in \mathcal{N}, j \notin \mathcal{Q} \tag{8}$$

Priority-Based Rerouting: Disrupted nodes with higher traffic should have higher priority for rerouting, i.e.,

$$\sum_{j\in\mathcal{N}} x^{i_1,j} + \sum_{k\in\mathcal{M}} \sum_{j\in\mathcal{N}} x^{i_1,k,j} \geq \sum_{j\in\mathcal{N}} x^{i_2,j} + \sum_{k\in\mathcal{M}} \sum_{j\in\mathcal{N}} x^{i_2,k,j} \quad ;\forall i_1, i_2 \in \mathcal{Q}, \text{ if } \mathcal{Q}_v^{i_1} \geq \mathcal{Q}_v^{i_2} \tag{9}$$

Flow Conservation: The flow into each intermediate node must equal the flow out of that node, i.e.,

$$\sum_{i\in\mathcal{Q}} x^{i,k} = \sum_{j\in\mathcal{N}} x^{k,j} \quad ;\forall k \in \mathcal{M} \tag{10}$$

Non-Negativity of routing variables: Ensure that the number of vehicles routed is non-negative, such that

$$x^{i,j} \geq 0 \quad ;\forall i \in \mathcal{Q}, j \in \mathcal{N}, j \notin \mathcal{Q}, \tag{11}$$

$$x^{i,k,j} \geq 0 \quad ;\forall i \in \mathcal{Q}, k \in \mathcal{M}, j \in \mathcal{N}, j \notin \mathcal{Q} \tag{12}$$

C. EVR-DC Algorithm

The EVR-DC algorithm uses an LP solver to optimize EV rerouting under disruptions. Optimal weights w_1, w_2, and w_3 are determined using the AHP by normalizing matrices for distance, traffic-to-capacity ratio, and route capacity. Based on five days of EVCS data, multiple weight combinations are generated, and the one minimizing Eq. 5 is selected. The EVR-DC algorithm, which integrates the AHP-derived weight values, is detailed in Algorithm 1. For each disrupted hour h, the algorithm retrieves the set of functional nodes $\mathcal{N}$ along with their available capacities $\mathcal{N}_c$. It then initializes an empty list, f, to store the rerouting satisfaction rate $\mathcal{R}^i$ values for each i. For every disrupted EVCS node $i \in \mathcal{Q}$ and each functional node $j \in \mathcal{N}$, the algorithm defines $\mathcal{N}^j$ as the set of allowed destination nodes, constrained to the routing decision within two hops. The hop restriction helps limit the solution space for traceability and ensures practical rerouting feasibility [28]. If $\mathcal{N}^j$ is empty, node i is skipped. Otherwise, the LP model is formulated for node i with decision variables $x^{i,j}$ for each $j \in \mathcal{N}^j$. The LP model minimizes the total routing objective function $\mathcal{U}$ while ensuring demand fulfillment, node and route capacities, rerouting priorities, flow conversion, and non-negativity, as enforced by constraints in

Algorithm 1: EVR-DC Algorithm

Input: $\mathcal{Q}, \mathcal{N}, \mathcal{N}_c$
Output: $\bar{\mathcal{R}}^i$
for *each disrupted hour* h **do**
  Retrieve $\mathcal{N}$ for hour h and capacities $\mathcal{N}_c$;
  Initialize f as an empty list;
  for *each* $i \in \mathcal{Q}$ *and* $j \in \mathcal{N}$ **do**
    Define $\mathcal{N}^j$ as nodes within 2 hops;
    if $\mathcal{N}^j$ *is empty* **then**
      Skip node i;
    end
    Formulate LP model for node i;
      Objective: Minimize $\mathcal{U}$ (Eq. 5);
      Decision: $x^{i,j}$ for each $i \in \mathcal{Q}^i$;
      Constraints: Eqs. 6, 7, 8, 9, 10, 11, and 12;
    Solve the LP model;
    if *model is infeasible* **then**
      Set EV not rerouted;
    else
      Compute $\mathcal{R}$ using Eq. 13;
    end
    Append $\mathcal{R}$ to f;
    Update $\mathcal{N}_c \leftarrow \mathcal{Q}_v^i$;
  end
  Compute $\bar{\mathcal{R}}^i$ using Eq. 14;
end

Eqs. 6 – 12. After solving the LP, if the solution is infeasible, it indicates that no valid rerouting paths are available, resulting in no EVs being rerouted; otherwise $\mathcal{R}^i$ is calculated as

$$\mathcal{R}^i = \frac{\sum_{i \in \mathcal{Q}} \sum_{j \in \mathcal{N}} x^{i,j}}{\mathcal{Q}_v^i}. \tag{13}$$

The R^i values are appended to f. The available capacities $\mathcal{N}^j$ for each node $j \in \mathcal{N}$ are updated by subtracting the allocated $x^{i,j}$. We compute the average rerouting satisfaction as

$$\bar{\mathcal{R}}^i \leftarrow \frac{1}{|f|} \sum_{\mathcal{R} \in f} \mathcal{R}^i. \tag{14}$$

V. Experimental Result

We evaluate the EVR-DC algorithm using two considerations: (i) capacity utilization change, measuring congestion reduction at disrupted EVCS and increased utilization at nearby EVCS within an hour, and (ii) the average yearly EV user rerouting satisfaction rate. To visualize the 305 EVCS capacity patterns, we apply K-means clustering into 31 geographic zones. Fig. 3 displays the zone distribution and disruption status at 7:00 AM on January 30, 2023, where disruptions at the 10 highest-traffic EVCS affected 3,379 EVs.

A. Congestion Reduction in Disrupted EVCS

According to Fig. 3, the disrupted EVCSs on January 30, 2023, at 7:00 AM are $S199$, $S175$, $S269$, $S104$, $S6$, $S48$,

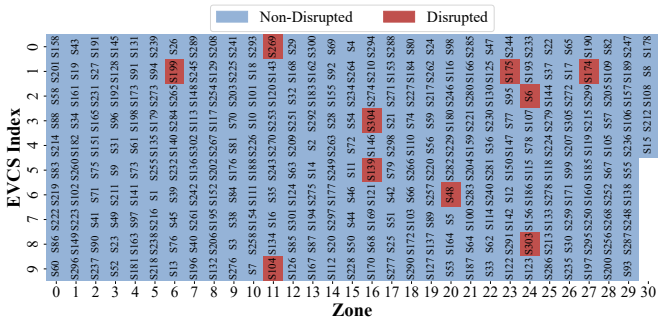

Fig. 3. Disrupted and non-disrupted EVCS at 7:00 AM January 30, 2023

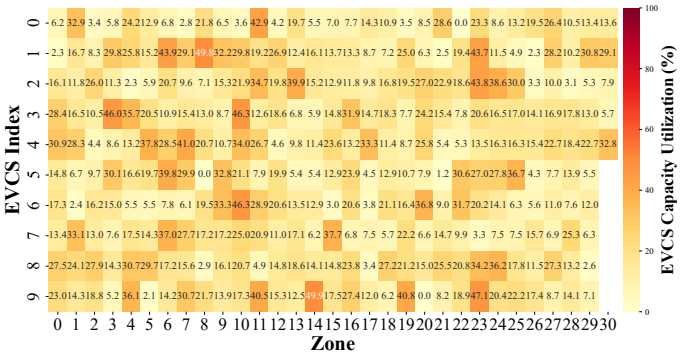

Fig. 4. Before rerouting EVCS utilization at 7:00 AM, January 30, 2023

$S303$, $S304$, $S174$, and $S139$. Their corresponding EVCS capacity utilization are 43.91%, 43.68%, 42.92%, 40.54%, 38.60%, 36.84%, 36.24%, 31.93%, 28.15%, and 23.86%, respectively. Fig. 4 shows the pre-rerouting capacity utilization, where lighter hues indicate lower and brighter hues indicate higher utilization. The EVR-DC algorithm processes disrupted EVCSs in descending order of traffic density, reducing congestion at disrupted EVCSs and rerouting EVs to nearby functional ones. As shown in Fig. 5, EVCS $S303$ (initially at 36.24%) had 90% of its 351 EVs rerouted 241 EV to $S73$ and 110 EV to $S257$ lowering its utilization from 36.24% to 3.62%. The utilization at $S73$ and $S257$ increased from 16.59% to 66.59% and 16.43% to 42.25%, respectively. Similarly, the load at $S269$ dropped from 42.92% to 4.26% after rerouting 242, 66, and 36 EVs to $S120$, $S253$, and $S270$, raising their utilization to 73.82%, 64.56%, and 54.19% from 34.73%, 12.59%, and 26.71%, respectively. No feasible rerouting was found for $S104$, so its utilization remained at 40.54%. Thus resulting the disrupted station congestion by 73.01% in an hour.

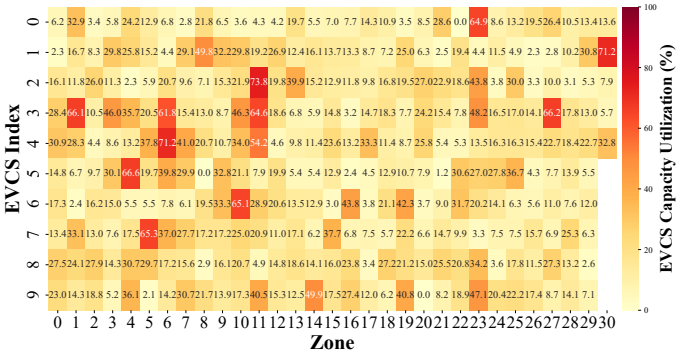

Fig. 5. After rerouting EVCS utilization at 7:00 AM, January 30, 2023

TABLE II
MONTHLY USER SATISFACTION RATE FOR THE YEAR 2021-2023

Month	EV Users Rerouting Satisfaction Rate		
	Y-2021	Y-2022	Y-2023
January	84.27%	86.72%	86.13%
February	85.58%	85.80%	85.62%
March	85.54%	85.34%	85.95%
April	85.86%	84.54%	86.44%
May	84.84%	84.22%	87.20%
June	84.70%	85.88%	86.56%
July	84.24%	85.92%	87.38%
August	85.27%	84.85%	87.86%
September	85.70%	86.11%	86.48%
October	84.84%	84.70%	86.54%
November	84.11%	85.26%	85.28%
December	86.67%	86.90%	84.69%

B. EV User Rerouting Satisfaction Rate

Table II presents the EV rerouting user satisfaction rate, highlighting the robustness and efficiency of the EVR-DC algorithm in dynamically managing disruptions within the EVCS network. Notably, the algorithm consistently achieves high satisfaction rates, with averages of 85.14%, 85.52%, and 86.34% in the years 2021, 2022, and 2023, respectively, which yield an overall yearly satisfaction rate of 85.67%. These results demonstrate that the EVR-DC algorithm meets the majority of rerouting demands even under varying network conditions and disruption intensities. Furthermore, the EVR-DC algorithm exceeds the average rerouting satisfaction rate in 12 out of 36 months further confirms its resilience, maintaining high satisfaction under disruptions and efficiently balancing the load between disrupted and functional EVCSs

VI. CONCLUSION

This paper introduced a graph-based rerouting strategy for EVs that dynamically reroutes them from disrupted EVCSs to functional EVCSs. The proposed EVR-DC algorithm, validated using real-world traffic data and a synthetic power bus model, not only reduced the congestion on disrupted EVCSs by up to 73% within an hour but also maintained an overall EV user rerouting satisfaction rate of 86%. Our outcomes highlight the algorithm's capability to balance utilization across the EVCS network as well as ensuring EVCS resilience under diverse operating conditions. Future research could develop machine learning–based rerouting systems to detect disrupted EVCS.

REFERENCES

[1] S. R. Fahim *et al.*, "Graph autoencoder-based power attacks detection for resilient electrified transportation systems," *IEEE Trans. on Transportation Electrification*, vol. 10, no. 4, pp. 9539–9553, Dec 2024.

[2] X. Tang *et al.*, "Distributed routing and charging scheduling optimization for internet of electric vehicles," *IEEE Internet of Things J.*, vol. 6, no. 1, pp. 136–148, Oct. 2019.

[3] M. R. Ahasan *et al.*, "Securing EVCS infrastructure against cyberattacks with a deep learning-based detection model," in *2025 10th International Conference on Fog and Mobile Edge Computing (FMEC)*. Tampa, FL, USA, 19-22 May 2025, pp. 33–38.

[4] Şükrü İmre *et al.*, "Understanding barriers and enablers of electric vehicles in urban freight transport: Addressing stakeholder needs in turkey," *Sustainable Cities and Society*, vol. 68, p. 102794, Mar. 2021.

[5] S. R. Fahim *et al.*, "Dynamic spatio-temporal planning strategy of ev charging stations and dgs using gcnn-based predicted power demand," *IEEE Trans. on Intelligent Transportation Systems*, vol. 26, no. 4, pp. 4528–4542, April 2025.

[6] B. Al-Hanahi *et al.*, "Charging infrastructure for commercial electric vehicles: Challenges and future works," *IEEE Access*, vol. 9, pp. 121 476–121 492, Aug. 2021.

[7] A. Takiddin *et al.*, "Generalized graph neural network-based detection of false data injection attacks in smart grids," *IEEE Trans on Emerging Topics in Comp. Intelligence*, vol. 7, no. 3, pp. 618–630, June 2023.

[8] R. Atat *et al.*, "Graphon neural networks-based detection of false data injection attacks in dynamic spatio-temporal power systems," *IEEE Open Access Journal of Power and Energy*, vol. 12, pp. 24–35, Jan. 2025.

[9] D. Aguiari *et al.*, "Monitoring electric vehicles on the go," in *2022 IEEE 19th Annual Consumer Communications Networking Conference (CCNC)*. Las Vegas, NV, USA, 08-11 Jan. 2022, pp. 885–888.

[10] H. B. School, "The state of ev charging in america," tinyurl.com/ev-charging-america, accessed: Nov. 2025.

[11] Electrify America LLC, "Electrify america mobile app," tinyurl.com/ev-mobile-app, accessed: Nov. 2025.

[12] J. Lin *et al.*, "Electric vehicle routing problem," *Transportation Research Procedia*, vol. 12, pp. 508–521, Feb. 2016.

[13] B. M. Portela *et al.*, "Cheapest insertion and disruption of routes operators for solving multi-depot electric vehicle location routing problem with time windows and battery swapping via GRASP and RVND," in *IEEE Congress on Evo. Comp.* Kraków, Poland, 28 June – 01 July 2021, pp. 2133–2140.

[14] A. Phu-ang *et al.*, "Modified genetic algorithm with flexible crossover for the capacitated electric vehicle routing problem," in *Int. Conf. on IT and Elec. Eng.* Chiang Mai, Thailand, 26–27 Oct. 2023, pp. 1–4.

[15] Q. Wang *et al.*, "Optimization of electric vehicle routing problem using tabu search," in *Chinese Control And Decision Conf. (CCDC)*. Hefei, China, 22-24 Aug. 2020, pp. 2220–2224.

[16] S. Hulagu *et al.*, "Electric vehicle location routing problem with vehicle motion dynamics-based energy consumption and recovery," *IEEE Trans. on Intell. Transp. Sys.*, vol. 23, no. 8, pp. 10 275–10 286, Jul. 2022.

[17] E. Messaoud, "A chance constrained programming model and an improved large neighborhood search algorithm for the electric vehicle routing problem with stochastic travel times," *Evolutionary Intelligence*, vol. 16, no. 1, pp. 153–168, Aug 2023.

[18] E. Winarno *et al.*, "Location based service for presence system using haversine method," in *Int. Conf. on Innovative and Creative Information Technology (ICITech)*. Salatiga, Indonesia, 02–04 Nov 2017, pp. 1–4.

[19] Federal Highway Adminstration, "Traffic Monitoring and Analysis System Dataset," tinyurl.com/trafficTMAS, [Online: Accessed Nov. 2025].

[20] European Automobile Manufacturers Association, "Electric Car Use by Country," tinyurl.com/EV-car-use, [Online; Nov. 2025].

[21] Visit Norway, "Plug-in Electric Vehicles in Norway," https://tinyurl.com/ev-norway-cars, [Online; Accessed Nov. 2025].

[22] H. Li *et al.*, "The creation and validation of load time series for synthetic electric power systems," *IEEE Trans. on Power Systems*, vol. 36, no. 2, pp. 961–969, Aug. 2021.

[23] U.S. Energy Information Administration, "Texas - state energy profile analysis," tinyurl.com/texas-eia, [Online: Accessed Nov. 2025].

[24] EV Database, "Tesla model 3," tinyurl.com/Tesla-battery-capacity, [Online: Accessed Nov. 2025].

[25] M. C. Ho *et al.*, "Collaborative vehicle rerouting system with dynamic vehicle selection," *IEEE Trans. on Intelligent Transportation Systems*, vol. 24, no. 12, pp. 14 546–14 555, Aug. 2023.

[26] F. Wang *et al.*, "Data-driven vulnerability analysis of shared electric vehicle systems to cyberattacks," *Transportation Research Part D: Transport and Environment*, vol. 135, p. 104379, Aug 2024.

[27] C. H. Babu *et al.*, "Optimizing power and energy loss reduction in distribution systems with rdgs, dsvcs and evcs under different weather scenarios," *Sust. Energy Tech. and Assesst.*, vol. 75, p. 104219, Jan. 2025.

[28] R. Shahbazian *et al.*, "Integrating machine learning into vehicle routing problem: Methods and applications," *IEEE Access*, vol. 12, pp. 93 087–93 115, Jul 2024.

[29] Q. Huang, "Evcs optimal planning based on dynamic traffic network charging demand prediction," in *Int. Conf. on Power and Renewable Energy (ICPRE)*. Guangzhou, China, 20-23 Sept. 2024, pp. 1502–1507.